UDK 621.313.33 **doi: 10.20998/2079-3944.2026.1.05**

S. DZENIS, V. BOLYUKH

ANALYSIS OF THE TEMPERATURE FIELD OF A HIGH-EFFICIENCY INDUCTION MOTOR

Introduction. In high-power induction motors, the problem of heat removal arises due to the increased density of losses in active elements. The preferred method of cooling induction motors is air cooling. An effective way to study the thermal state of an induction motor is the theoretical calculation of interdependent electromagnetic and temperature fields with experimental verification of the calculation results. **Purpose and objectives**. Determination and analysis of the three-dimensional temperature field of a high-efficiency induction motor using two-dimensional mathematical models and experimental measurement of the outer surface using a thermal imaging camera. **Methods.** Using interconnected two-dimensional electromagnetic models and three thermal submodels representing the stator slot segment and the central radial and axial sections, the three-dimensional magnetic field of a high-efficiency induction motor was reconstructed and experimentally validated. **Results**. The calculation of the electromagnetic field that determines the distribution of heat sources in the motor was performed. The temperature field is found iteratively by matching the temperature fields in the stator slot segment, in the central radial and axial sections of the motor with corrected thermophysical parameters. **Conclusions**. Measurement of the temperature of the electric motor housing using a thermal imaging camera confirmed the reliability of theoretical calculations. The relative error between the calculated and measured temperature values on the outer surface of the induction motor housing is 2-6%.

Keywords: induction motor, two-dimensional mathematical models, electromagnetic field, temperature field, experimental studies, thermal imaging camera.

С.Е. ДЗЕНИС, В.Ф. БОЛЮХ

АНАЛІЗ ТЕМПЕРАТУРНОГО ПОЛЯ ВИСОКОЕФЕКТИВНОГО АСИНХРОННОГО ДВИГУНА

Вступ. В асинхронних двигунах високої потужності виникає проблема відведення тепла через підвищену густину втрат в активних елементах. Переважним методом охолодження асинхронних двигунів є повітряне охолодження. Ефективним способом дослідження теплового стану асинхронного двигуна є теоретичний розрахунок взаємозалежних електромагнітних та температурних полів із експериментальною верифікацією результатів розрахунку. **Мета та завдання.** Визначення та аналіз тривимірного температурного поля високоефективного асинхронного двигуна за допомогою двовимірних математичних моделей та експериментальний вимір зовнішньої поверхні за допомогою тепловізійної камери. **Методи.** За допомогою взаємопов'язаних двовимірних моделей електромагнітного поля та трьох моделей температурного поля у сегменті паза статора, у центральних радіальному та аксіальному перерізі визначено тривимірне магнітне поле високоефективного асинхронного двигуна з експериментальним підтвердженням достовірності. **Результати.** Виконано розрахунок електромагнітного поля, що визначає розподіл джерел тепла у двигуні. Температурне поле знаходиться ітераційним способом шляхом узгодження температурних полів у сегменті паза статора, в центральних радіальному та аксіальному перерізах двигуна при коригуванні теплофізичних параметрів. **Виводи.** Вимірювання температури корпусу електродвигуна за допомогою тепловізійної камери підтвердили достовірність теоретичних розрахунків. Відносна похибка між розрахованими та виміряними значеннями температур на зовнішній поверхні корпусу асинхронного двигуна становить 2-6 %.

Ключові слова: асинхронний двигун, двомірні математичні моделі, електромагнітне поле, температурне поле, експериментальні дослідження, тепловізійна камера.

Introduction. When designing high-speed, high-power induction motors (IMs), the problem of heat dissipation arises due to the high density of losses in the motor's active components [1]. The resulting temperature increases affect the motor's service life and performance and can lead to failure. The heat generated during operation negatively affects the motor's efficiency, can cause the motor to overheat, degrade the insulation of the windings, and potentially lead to a short circuit. Therefore, it is necessary to control the thermal processes of these motors to ensure reliability and improve performance [2]. Reducing the overheating temperature of the stator windings and rotor bars can be achieved by improving the cooling of its active elements and reducing losses. In this context, the application of cryogenic cooling of the windings is being investigated, which can even improve the performance of the electric motor [3].

Thermal analysis is a critical stage in the design of electric machines [4, 5]. It helps develop effective thermal monitoring methods, provides a better understanding of the motor's overall performance, and prevents equipment failure. Temperature measurement in electric motors is crucial for protecting components from overheating and for maximizing their power and torque output. Since direct measurement involves costs and integration challenges, model-based temperature estimation methods are becoming increasingly important. These methods can be categorized into indirect methods that track temperature-sensitive motor parameters, direct methods based on thermal networks with concentrated parameters, and machine learning methods [6, 4].

Various methods are used to cool induction motors, including cryogenic cooling, hydrogen cooling, heat pipes, and the use of phase-change materials [7]. It is noted that it is advisable to use a combination of different cooling methods for individual motor parts, as they are subjected to uneven thermal loads. This allows the temperature within the motor to be regulated, which increases the torque and efficiency of the motors.

Using the heat transfer coefficient and maximum heat flux as key performance indicators, this study examines indirect and direct air cooling, jacket cooling, spray cooling, heat pipe cooling, flood cooling, immersion cooling, inter-turn cooling, intra-turn cooling, and cooling using phase-change materials [8].

However, the predominant method of cooling asynchronous motors is air cooling using external fins, air ducts, air gaps, and fan impellers [9]. Internal cooling using rotor and stator air ducts, along with optimized duct geometry, demonstrates the potential to increase the power-to-size ratio and reduce motor dimensions. In contrast, liquid cooling systems provide a power-to-weight ratio of up to 25 kW/kg, achieved through stator heat exchangers and cooling tubes. In [10], it is shown that for an induction motor, water cooling reduced operating temperatures by 39.49% at the end windings, by 41.67% at the side

windings, and by 56.95% at the stator core of the induction motor compared to air cooling. However, liquid cooling systems are complex, require maintenance, and demand a high degree of protection against moisture and dust ingress.

This paper examines effective methods for regulating the temperature of an induction motor [11]. Particular attention is paid to energy losses, hot spots, the effect of overheating on motor efficiency, various cooling strategies, specific experimental approaches, and power control methods. The method of concentrated parameter schemes and the finite element method for thermal analysis and various cooling strategies are discussed.

Using temperature measurements with thermocouples, a thermal analysis of the motor is performed in real time, taking into account the operating cycle [12]. The highest temperature is observed at the end windings due to the low heat transfer rate through the winding insulation and air gap. Introducing a channel for fluid flow increases the heat transfer rate, and the temperature of the end winding can be reduced by up to 15%.

Using three-dimensional computational fluid dynamics, the thermal behavior of motors with fully enclosed fan cooling is investigated [13]. A realistic stator geometry with cooling channels is considered, and rotor rotation is taken into account. Measured airflow data are used to simulate the air velocity in the cooling channels. The loss distribution is obtained using a transient electromagnetic finite element model. The boundary conditions employ a model of total radiation along with natural convection.

Problem Statement. An increase in motor temperature is closely related to its operating conditions. When the motor is overloaded, the current in the windings can lead to localized overheating of the windings, which jeopardizes the safe operation of the motor. To determine the heating state of an induction motor under various operating conditions, a three-dimensional thermal model of the motor was developed to calculate the transient rise in motor temperature under normal operating conditions and typical winding fault conditions [14]. Using this model, the influence of operating conditions on the motor's thermal characteristics was investigated.

A mathematical model with concentrated parameters is used to determine the temperature distribution inside an induction motor, assess its thermal stability, and verify the insulation of copper windings under various operating conditions [15]. Analysis of the thermal model showed that the most heated elements in an induction motor are the end windings and the rotor bars. This is due to losses in the stator copper and losses in the rotor bars, which depend on the stator current. The stator current can increase due to an increase in torque or a decrease in stator frequency, which leads to a rise in the temperature of each element. The thermal model of the induction motor was verified by comparing the calculated temperatures of each element with experimental results obtained using thermocouples connected to a computer via a data logger.

Various thermal analysis methods are employed, including the finite element method, a thermal network with concentrated parameters, and computational fluid dynamics tools, across different cooling strategies. An integrated approach utilizing two or more cooling strategies allows for combining the advantages of individual systems while compensating for their shortcomings [2]. For motor analysis, a combined electromagnetic, mechanical, and thermal calculation is performed using modern CAD tools based on two-dimensional finite element models [16, 17].

Using the ANSYS Motor-CAD program, the temperature field of an induction motor was constructed, and the effectiveness of using nanofluids as a cooling medium was investigated [18]. It was found that the thermal conductivity of nanofluids exceeds that of traditional cooling media, such as air and water. Nanofluid can significantly improve motor efficiency, thereby reducing temperature rise and increasing system efficiency. The use of CuO nanofluid as a cooling medium in an induction motor resulted in a 10% reduction in motor housing temperature.

Based on a physical model of flow in the internal and external air ducts, the flow patterns and pressure distribution were determined, boundary conditions for calculating the coupled thermal field were established, and the temperature distribution inside the machine was obtained [19]. Thus, effective ventilation increases power output while reducing the motor's mass and energy consumption.

For a high-power motor with high torque and rotational speed, a cooling mechanism integrated into the motor rotor is proposed [1]. It consists of six channels inside the hollow shaft, through which air is drawn in by the centrifugal force of the rotating rotor. The proposed mechanism creates an airflow inside the motor; its velocity increases proportionally to the rotational speed, convective heat transfer improves, and the temperature of hot spots decreases. However, this system is ineffective at speeds below 5,000 rpm.

To address the issue of overheating in high-efficiency high-voltage motors caused by high power density and electromagnetic load, a flow network was developed to predict temperature and analyze motor energy efficiency [20]. To this end, local 3D fluid-solid interaction models were created, which are effectively linked to the global fluid flow network of the motor via fluid pressure. The model is used to find an optimized design that improves cooling by varying the height of the air deflectors and adjusting their number. The maximum temperature of the stator and rotor of the internal ventilated channel, as well as the temperature at the outlet of the internal ventilated channel, are reduced, which allows for a further increase in the motor's power output.

A comparison of various approaches to studying thermal phenomena in induction motors is conducted [21]. In the first approach, temperature-dependent material properties were used, and changes in the power supply current were taken into account. The second approach was independent of temperature throughout the entire simulation. This eliminates calculation errors caused by the variability of air thermal conductivity. This method allows for a reduction in the number of elements in the final model, since the air in the air gap is not meshed, which leads to a reduction in computation time.

An approach is proposed for the fast and efficient real-time estimation of the rotor temperature in an induction motor [22]. It consists of three stages: 1) converting nonlinear differential equations into discrete algebraic equations based on measured voltage and current, 2) obtaining

approximate analytical solutions for the rotor resistance and stator inductance, which are used to estimate the rotor temperature, 3) development of a general procedure for obtaining approximate analytical solutions to nonlinear differential equations. Experimental results show that the method provides a minimum estimation error, which complies with the standards established by IEC 60034-2-1.

The effect of poor-quality electrical power on the operating temperature conditions of an induction motor is investigated [23]. Experimental and analytical dependencies of the motor temperature change over time when connected to a supply voltage with various sinusoidal distortion coefficients are presented.

Thus, currently the most effective method for studying the thermal state of an induction motor is the theoretical calculation of interrelated electromagnetic fields with experimental verification of the calculation results. The most effective computational models describe the 3D configuration of an induction motor. However, such models require significant computational resources and powerful computer hardware.

The most effective experimental methods involve measuring the temperatures of the hottest motor components. Since these components are located inside the motor block, significant challenges arise when attempting to install appropriate temperature sensors in them.

Purpose and Objectives. To determine and analyze the three-dimensional temperature field of a high-efficiency induction motor using two-dimensional mathematical models and to experimentally measure the outer surface using a thermal imaging camera.

Scientific novelty. Using an interconnected two-dimensional electromagnetic field model and three temperature field models in the stator slot segment, at the central radial and axial cross-sections, the three-dimensional magnetic field of a high-efficiency asynchronous motor was determined with experimental validation of its accuracy.

Problem Statement. Consider the temperature field of a prototype three-phase squirrel-cage motor connected to a power grid with a frequency of $f_s = 50$ Hz, which has a rated power of $P_N = 110$ kW, a shaft height of 280 mm, and a pole pair number of p = 2. This motor has outer diameters of the rotor core $d_r = 237.8$ mm and the stator $d_s = 420$ mm, their length $l_a = 340$ mm, and an air gap of 1.1 mm. The stator has $Q_s = 48$ slots, and the rotor has $Q_r = 40$ slots. The stator winding is a two-layer, diametrical, distributed winding. The closed rotor slots are chamfered at 2.9°. The core material is M400-50A steel. This fully enclosed motor with a cast iron housing and low-pressure fan cooling is designed to achieve IE3 energy efficiency (Fig. 1). The results of the motor test according to the protocol are presented in Table 1.

Let us consider the steady-state electromagnetic and thermal processes during the motor's rated operating mode. We examine the electromagnetic field in a cross-section of the motor's active zone.

Fig. 1. Prototype of a three-phase induction motor during testing

Table 1 – Motor test results

Electrical power P_1	115,729 kW,
Mechanical power P_2	110,313 kW
Voltage U_1	401 V
Rated current I_1	184,2 A
No-load current I_0	37,15 A
Power factor cos φ	0,905
Rotational speedn_2	2979,87 rpm
Torque M_2	352,92 Nm
Efficiency η	95,32 %
Winding temperature rise θ_1	69,8 °C
Rear bearing temperature T_r	26,1 °C
Front bearing temperature T_f	30,0 °C

A two-dimensional computational model was adopted for numerical field studies using the ANSYS Motor-CAD software [24]. The motor computational model represents its design and incorporates the distribution and directions of currents in the windings, as well as the magnetic properties of the cores. The program uses polar coordinates r, α. The directions of the rotor rotational frequency n_r and the stator magnetic field n_s coincide with the direction of the α coordinate.

The currents in the stator phase windings are defined as:

$$i_{sA} = I_{ms}\cos(\omega_s t);\ i_{sB} = I_{ms}\cos(\omega_s t - \tfrac{2}{3}\pi);$$
$$i_{sC} = I_{ms}\cos(\omega_s t + \tfrac{2}{3}\pi), \quad (1)$$

where $I_{ms} = \sqrt{2}\cdot I_s$ – current amplitude; I_s – their rms value; $\omega_s = 2\pi f_s$ – angular frequency; t – time.

The phase currents of the stator winding are specified at time t=0, so their instantaneous values are given by: $i_{sA} = I_{ms}$, $i_{sB} = i_{sC} = -0{,}5I_{ms}$.

The ANSYS Motor-CAD software employs a lumped-parameter thermal network approach combined with analytical and empirical correlations to evaluate heat transfer in the motor. Finite element methods are applied locally, where necessary, to refine thermal parameters in complex regions such as the stator slot.

For the electromagnetic field analysis, a two-dimensional finite element formulation is used, governed by the following equation:

$$\mathrm{rot}\left[\frac{1}{\mu(B)}\mathrm{rot}(\vec{k}A_z)\right] = \vec{k}J_z, \quad (2)$$

where J_z, A_z are the axial components of the current density vector and the magnetic potential vector; $\vec{k}$ – the unit vector of the z-axis; μ – magnetic permeability: either the magnetic constant μ_0 for non-magnetic regions, or determined for the magnetic flux density B along the core's

magnetization curve.

Equation (2) is supplemented by a boundary condition – the value of the vector magnetic potential at the boundary of the computational domain. A homogeneous first-kind boundary condition is specified at the outer boundary of the stator core, accounting for the absence of stray magnetic fluxes on the stator yoke.

As a result of solving Equation (2) using the ANSYS Motor-CAD program, we obtain the distribution of the vector magnetic potential A_z and the magnetic field induction B in the cross-section of the motor (Fig. 2). After solving Equation (2), the components of the magnetic induction are determined using the known values of the vector magnetic potential

$$B_x = \partial A_z / \partial y;\ By = \partial A_z / \partial x. \qquad (3)$$

The results of the calculation of the two-dimensional magnetic field in the cross-section of an induction motor are shown in Fig. 2.

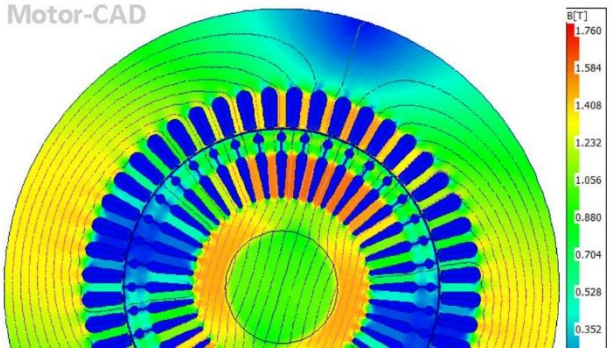

Fig. 2. Magnetic field distribution in the cross-section of an induction motor

Power losses in the stator winding and core are calculated using conventional methods. Losses in the stator winding:

$$p_1 = 3I_s^2 R_1(T), \qquad (4)$$

where $R_1(T)$ is the active resistance of the stator winding phase.

We neglect iron losses in the rotor core, while losses in the stator yoke and teeth are calculated using empirical formulas [25]:

$$p_j = p_{1/50}(0{,}02\,f)^{1{,}5} k_j B_j^2 m_j, \qquad (5)$$

where $j=a, z$ – are the indices of the yoke and stator teeth, respectively; k_j are coefficients accounting for non-uniformities in the magnetic flux distribution; B_j – average values of magnetic induction; m_j – masses of ferromagnetic elements; $p_{1/50}$ – specific loss value at 1 T induction and 50 Hz frequency.

Specific power losses in the stator winding, the stator yoke, and the stator teeth:

$$Q_1 = p_1 / V_1;\ Q_{a_1} = p_a / V_a;\ Q_{z_1} = p_z / V_z, \qquad (6)$$

where V_1, V_a, V_z are the volumes of the stator winding conductors, the yoke, and the stator teeth, respectively.

Based on equations (1)-(6), the parameters of the induction motor are calculated, which are used to determine its temperature field.

Mechanical friction losses accounted for in the model are introduced in the form of equivalent power losses due to friction in the bearings, aerodynamic losses in the ventilation unit, and friction between the rotor surface and the air, as well as in the shaft seals (if present in the design).

Thus, the electromagnetic calculation of an induction motor allows determining the distribution of losses, which are introduced into the thermal model as heat sources.

The thermal field of an induction motor can be described by a steady-state heat conduction differential equation in Cartesian coordinates [26]:

$$\lambda(T)\left[\frac{\partial^2 T(x,y)}{\partial x^2} + \frac{\partial^2 T(x,y)}{\partial y^2}\right] = -Q(x,y), \qquad (7)$$

where $\lambda(T) = \lambda_0(1+\beta_T \Delta T)$ – the temperature-dependent thermal conductivity coefficient, β_T – an experimentally determined constant.

Third-order boundary conditions are imposed on the outer boundaries of the computational domain and on the surfaces of the ventilation ducts:

$$\lambda(T)\frac{\partial T}{\partial n} = -h(\nu)(T - T_{0x}), \qquad (8)$$

where $h(\nu)$ is the heat transfer coefficient from surfaces, which depends on the cooling air flow velocity ν; T_{0x} is the average temperature of the cooling air, determined by taking into account its heating as it flows through the cooled channel.

On the outer surfaces of the casing, fins, end plates, and protruding structural elements, the heat transfer coefficient was specified locally with different values depending on the surface area.

Detailed boundary conditions were applied to the finned surface of the housing. The inner contour of the fin on the side facing the inter-fin channel and the outer contour of the fin were assigned different heat transfer coefficients.

Each fin was divided along its length into sections, each of which was assigned its own heat transfer coefficient. Thus, the heat transfer coefficient was specified as a piecewise-constant function of the coordinate, which allowed for changes in airflow conditions along the fin's length and differences in heat exchange on its inner and outer surfaces.

A combined approach was used when specifying boundary conditions on the surfaces of the end plates and the motor's internal cavities. For some surfaces, heat transfer was determined by air thermal conductivity in the corresponding internal regions. For other surfaces, such as sections of the shields and structural elements, third-order boundary conditions with different heat transfer coefficients were applied.

The air gap was modeled as a region with the thermophysical properties of air, ensuring heat transfer via thermal conductivity, and a third-kind boundary condition was additionally applied to the outer surface of the rotor, which accounted for the intensification of heat transfer associated with the rotor's rotation.

In ANSYS Motor-CAD, the temperature field of an induction motor with a radial fan is calculated by accounting for heat transfer between the motor housing and the surrounding environment. The boundary conditions take into account convection, radiation, and air circulation.

For the outer surface of the housing, the boundary condition includes three heat transfer mechanisms: forced convection, natural convection, and radiation, which combine to form a single heat transfer coefficient.

Forced convection is accounted for during air cooling, and its magnitude is determined by the flow velocity generated by the radial fan and the geometry of the ducts:

$$V = V_r \cdot k_l \cdot n \cdot n_r^{-1}, \quad (9)$$

where V is the local air velocity; V_r is the reference velocity; k_l is the leakage coefficient; n, n_r are the current and reference rotational speeds, respectively.

For inter-fin channels, the heat transfer coefficient under forced convection [27]:

$$h_{forc} = 0,25 L_a^{-1} \rho C_p D_h V \left[1 - \exp(-m)\right], \quad (10)$$

where ρ is the air density; C_p is the specific heat capacity; D_h is the hydraulic diameter of the duct; L_a is the length of the duct; m – is a parameter defined as

$$m = 0,1418 \frac{L_a^{0,946}}{D_h^{1,16}} \left(\frac{\lambda_a}{\rho C_p V} \right)^{0,214}, \quad (11)$$

where λ_a – thermal conductivity of air.

These relationships determine the baseline heat transfer rate characteristic of the motor in question. To account for flow turbulence, a factor λ_{turb} is introduced to increase the heat transfer coefficient:

$$h_{forc}^{eff} = h_{forc} \lambda_{turb}, \ \lambda_{turb} = 1,7...1,9. \quad (12)$$

Natural convection is determined by the temperature difference between the motor casing surface and the surrounding environment, with a heat transfer coefficient

$$h_{nat} = Nu \cdot \lambda \cdot L_a^{-1}, \quad (13)$$

where is the is the $Nu = f(Gr \cdot \Pr)$ – Nusselt number, $Gr = g \cdot v^{-2} L_a^3 \beta (T_s - T_\infty)$ – Grashof number, $\Pr = C_p \lambda^{-1} \mu$ – Prandtl number, g – acceleration due to gravity; β – coefficient of volumetric expansion; T_s – surface temperature; T_∞ – ambient temperature; $v = \mu \cdot \rho^{-1}$ – kinematic viscosity; μ – dynamic viscosity.

The contribution of natural convection is determined by the current temperature level and becomes significant when the air flow velocity V decreases substantially.

Radiative heat transfer is included in the heat transfer boundary condition and is determined using the equivalent coefficient:

$$h_{rad} = \varepsilon \sigma \left(T_s^4 - T_\infty^4\right)\left(T_s - T_\infty\right)^{-1}, \quad (14)$$

where ε is the surface emissivity; $\sigma = 5,67 \cdot 10^{-8}$ W/(m²·K⁴). Radiative heat transfer is taken into account when calculating external heat transfer, regardless of the convection regime.

The total heat transfer coefficient, accounting for forced and natural convection with radiation:

$$h = h_{forc}^{eff} + h_{nat} + h_{rad}. \quad (15)$$

In the process of calculating the temperature field, the heat transfer coefficients are taken into account as follows: at each step of the iterative calculation, h_{nat} и h_{rad} are recalculated based on the current surface temperature T_s h_{forc}^{eff} is determined based on the specified flow velocity, and then the total coefficient h is calculated.

Thus, the motor's temperature field is determined by the combined action of forced and natural convection with radiation as part of a single heat transfer boundary condition. In this case, forced convection plays the dominant role, while the contribution of natural convection and radiation is determined by the current temperature regime and cooling conditions.

The heat transfer coefficient from the wall of a circular duct to the air is described by the relationship [26]:

$$\alpha(v) = 0,027 \lambda \cdot a^{-0,78} \cdot d_k^{-0,22} \cdot v^{0,78}, \quad (16)$$

where $\alpha = \lambda(T)/C_\rho = 2,4 \cdot 10^{-5}$ m²/s – thermal diffusivity of air at 40 °C; λ = 0.0267 W/m·°C – thermal conductivity of air at 40 °C; C_ρ = 1020 J/kg·°C – specific heat capacity; d_k – duct diameter. The flow velocity v_i in the i-th ventilation duct is expressed in terms of the cooling air flow rate P_i in the duct and the duct cross-sectional area s_i:

$$v_i = P_i / s_i, \quad (17)$$

An air-cooled induction motor includes ventilation ducts and various chambers. To move air, the fan generates a pressure H, which overcomes the system's aerodynamic resistance z at an air flow rate Q [25]:

$$H = zP^2 \quad (18)$$

Table 2 – Motor losses, kW

Electrical ΔP_e	1,55
Magnetic losses in the stator ΔP_{m1}	1,02
losses in the aluminum rotor cage ΔP_{m2}	0,761
Frictional ΔP_{mex}	1,36
Stray losses ΔP_d	0,72
Total losses ΔP	5,411

An iterative approach is used to determine the motor's temperature field, in which the values of the parameters for active materials, boundary conditions, heat losses, the magnetic field, and the temperature distribution are adjusted during the calculation process.

Results. Experimental tests of the specified motor were conducted on a special test bench, where various types of losses were determined (Table 2). The experimentally measured loss values agree with the calculated values to within 7-10%.

Since the temperature field in an induction motor is three-dimensional, three interconnected mathematical models were developed to simulate it using ANSYS Motor-CAD: one for the stator slot segment, one for the central radial cross-section, and one for the central axial cross-section of the motor (Fig. 3). This system of mathematical models allows the temperature field distribution along the electric motor housing to be calculated using an iterative method, taking fan cooling into account.

When calculating the temperature in the stator slot segment, its actual geometry and structure are taken into account, including copper conductors, insulation, a wedge, and an impregnation layer (Fig. 3a). Second-order boundary conditions are specified on the selected straight slot boundaries, and third-order boundary conditions on the outer and inner radial boundaries. This model allows for the calculation of the temperature in the insulation, which

is important for its reliability. The temperature is lowest on the outer surface of the stator housing, at approximately 64°C, while the temperature is highest on the inner surface of the stator, at approximately 97°C.

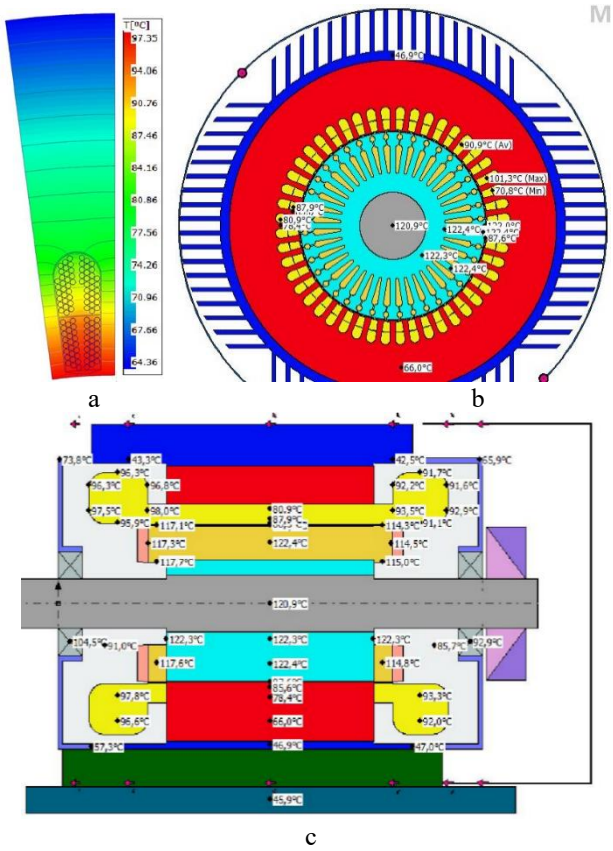

Fig. 3. Temperature distribution in the stator slot segment (a), in the central radial cross-section (b), and in the central axial cross-section (c) of the motor

When calculating the temperature in the central radial cross-section of an electric motor, the windings and tooth structures of the stator and rotor cores, the outer stator cooling fins, and the rotor shaft are taken into account (Fig. 3b). An increased concentration of mesh elements is specified in the air gap between the inner surface of the stator and the outer surface of the rotor.

In this model, the temperature is calculated at the corners of the frame, the tips and bases of the cooling fins, and at the points where the legs connect to the housing. However, this model uses averaged convection values, does not account for the bearing shields, and does not reflect temperature non-uniformities along the motor housing.

When calculating the temperature in the axial direction (Fig. 3c), one can estimate the temperature distribution along the axis: in the shaft, bearings, bearing shields, and fan. This model uses data from the segmented (Fig. 3a) and radial (Fig. 3b) models to refine the temperatures of the rotor and stator windings.

This model allows for the assessment of the thermal state of all machine components: the housing along the axis, taking into account changes in cooling and radiation conditions; the bearing shields; the bearings (taking into account mechanical losses); the shaft at the drive end, the shaft section under the rotor pack, the rotor pack itself and the rotor cage along its length, the end sections of the winding, the fan (taking into account fan losses), the rear shield, and the casing.

However, in this model, its thickness is equal to the thickness of a single frame rib. Inside the stator and rotor slots, the level of detail is limited, so refined data from previous models is used.

Thus, for an adequate assessment of the thermal state of an induction motor that accounts for the actual geometry of the machine, the physical properties of materials, and cooling conditions (including changes in convection and radiation), it is advisable to use a combination of interconnected models, each of which has its own advantages and disadvantages.

The slot segment model provides micro-detailing and identifies local overheating in the stator and rotor windings. The radial model reflects heat paths from the winding to the housing. The axial model shows the temperature distribution along the length of the machine, including the bearing assemblies.

The temperature field in an induction motor is determined iteratively by matching the temperature fields in the stator slot segment and in the central radial and axial cross-sections of the motor through the adjustment of thermophysical parameters.

The iterative coupling of the slot, radial, and axial models enables the reconstruction of the three-dimensional temperature field of the induction motor.

To verify the computational model, experimental studies were conducted by measuring the temperature of the electric motor housing using a “TiS60+ Fluke Thermography” thermal imaging camera (Fig. 4).

The results of the calculated and measured average temperatures at certain locations on the induction motor are presented in Table 3, where:
Section No. 1 – On the side surface of the ribs;
Section No. 2 – On the front bearing shield;
Section No. 3 – On top of the housing;
Section No. 4 – On the motor feet.

Table 3 – Results of calculated and measured average temperatures in motor sections

Section	Calculated	Measured	Measured
№ 1	43,9 ºC	42,6 ºC	2,9%
№ 2	73,8 ºC	78,3 ºC	6,1 %
№ 3	46,9 ºC	47,5 ºC	1,3 %
№ 4	45,9 ºC	35,9 ºC	21,7 %

A comparison of the calculated and measured average temperatures on the outer surface of the induction motor housing shows that the relative error is 2-6%, which is an acceptable result for verifying the computational model. The exception is a significant error of 21,7% at the motor feet and bearing assemblies. This significant difference can be explained by the fact that the induction motor is mounted on a base to which heat is dissipated from the motor legs, as well as by the use of an analytical model and a simplified calculation of heat dissipation from the bearings. Therefore, the measured temperature value is lower than the calculated value, where the motor is considered thermally isolated from external devices.

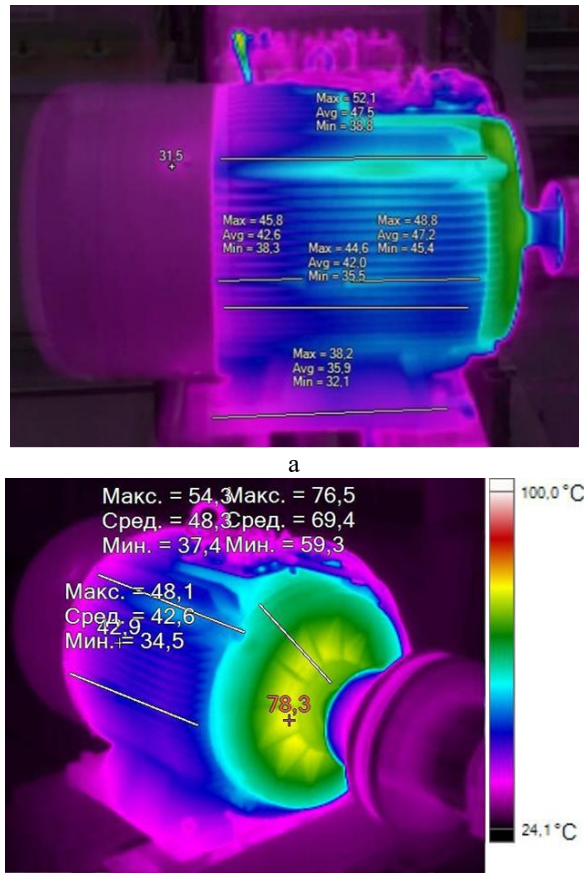

Fig. 4. Results of temperature measurements taken from the side (a) and the end of an electric motor housing using a thermal imaging camera

Thus, it can be concluded that the experimental results confirm the calculated results, which indicates the correctness of the proposed mathematical model.

Based on this, the calculation model is used to identify the hottest areas without installing special sensors inside the electric motor.

Conclusions. Using coupled two-dimensional electromagnetic and thermal models, the three-dimensional temperature field of a high-efficiency induction motor was reconstructed.

The electromagnetic field calculation provides the distribution of power losses, which are introduced into the thermal model as heat sources.

The temperature field in the induction motor is determined by an iterative method of matching the temperature fields in the stator slot segment, in the central radial and axial cross-sections of the motor, by adjusting the thermophysical parameters.

Experimental studies involving the measurement of the electric motor housing temperature using a thermal imaging camera confirmed the accuracy of the theoretical calculations. The relative error between the calculated and measured temperature values on the outer surface of the induction motor housing is 2-6%.

References

1. Awungabeh F.A., Besong J.E., Yasutaka F. Airflow Cooling Mechanism for High Power-Density Permanent Magnet Motor. IEEE Open Journal of the Industrial Electronics Society. (2024). pp. 1-14. https://doi.org/10.1109/OJIES.2024.3360509
2. S. Madhavan, R. Devdatta, E. Gundabattin. Thermal Analysis and Heat Management Strategies for an Induction Motor, a Review. Energies,2022, 15(21), 8127; https://doi.org/10.3390/en15218127
3. V.F. Bolyukh, N. Kryukova, I.I. Katkov. Influence of cryogenic temperature processes on the work of the linear pulse electromechanical converter // Refrigeration Science and Technology. – Vol. 2017-May, 2017, Pages 263-268
4. Ł. Nogal, A. Magdziarz, D. D. Rasolomampionona et al. The Laboratory Analysis of the Thermal Processes Occurring in Low-Voltage Asynchronous Electric Motors. Energies, (2021). 14. 2056. https://doi.org/10.3390/en14082056
5. L. Shao, A.Karci, D. Tavernini et al. Design Approaches and Control Strategies for Energy-Efficient Electric Machines for Electric Vehicles-A Review. IEEE Access. (2020), pp. 1-1. https://doi.org/10.1109/ACCESS.2020.2993235
6. O. Wallscheid Thermal Monitoring of Electric Motors: State-of-the-Art Review and Future Challenges. IEEE Open Journal of Industry Applications. (2021). pp. 1-1. https://doi.org/10.1109/OJIA.2021.3091870
7. Gundabattini, Edison & Solomon, Darius & Kalam, Akhtar & Kothari, D.P. & Bakar, Rosli. (2020). A review on methods of finding losses and cooling methods to increase efficiency of electric machines. Ain Shams Engineering Journal. 12. https://doi.org/10.1016/j.asej.2020.08.014
8. X. Li, X. Zhao, Z. Zhang et al. Selecting cooling methods for electric motors. Applied Thermal motorering 274 (2025) 126554. https://doi.org/10.1016/j.applthermaleng.2025.126554.
9. D. Konovalov, I. Tolstorebrov, T.M. Eikevik et al. Recent Developments in Cooling Systems and Cooling Management for Electric Motors. Energies, 2023, 16(19), 7006, https://doi.org/10.3390/en16197006
10. K. Y. Reddy, P. Vamsi, R. Peram. et al. Thermal Analysis and Cooling Strategies of High-Efficiency Three-Phase Squirrel-Cage Induction Motors-A Review. Computation. (2024). 12. 6. https://doi.org/10.3390/computation12010006
11. A. Boglietti, F. Mandrile, E. Carpaneto et al. Stator Winding Second-Order Thermal Model including End-Winding Thermal Effects. Energies. (2021).14. 6578. https://doi.org/10.3390/en14206578
12. R. Selvakumar, N. Sasikumar, R. Sathish et al. Thermal Analysis of an Electric Motor in an Electric Vehicle. Conference: WCX SAE World Congress Experience. SAE Technical Papers. (2023). https://doi.org/10.4271/2023-01-0532
13. K. K. Ronnberg, M. Beniakar. Thermal modelling of totally enclosed fan-cooled motors via conjugate heat transfer analysis and air-flow measurements. Conference: 2016 IEEE Conference on Electromagnetic Field Computation (CEFC). 2016. 1-1. https://doi.org/10.1109/CEFC.2016.7816290
14. Y. Xia, B. Ren, B. Jing et al. Analysis of transient temperature field of five-phase induction motor with composite winding under different operating conditions. Case Studies in Thermal motorering, Volume 63, 2024, 105402, https://doi.org/10.1016/j.csite.2024.105402.
15. O. O. Badran, H. Sarhan, B. Alomour. Thermal performance analysis of induction motor. International Journal of Heat and Technology. 2012, 30(1):75-88.
16. Młot, Adrian & Korkosz, Mariusz & Lechowicz, Andrzej & Podhajecki, Jerzy & Rawicki, Stanisław. Electromagnetic analysis, efficiency map and thermal analysis of an 80-kW IPM motor with distributed and concentrated winding for electric vehicle applications. Archives of Electrical motorering, (2022). 981-1002. https://doi.org/10.24425/aee.2022.142120
17. V.F. Bolyukh, O. I. Kocherga Efficiency of multi-armature linear pulse electromechanical power and speed converters. Electrical motorering & Electromechanics, 2024, no. 3, pp. 3-10. https://doi.org/10.20998/2074-272X.2024.3.01
18. G. K. Pandey, S. S. Sikha, A. Thakur et al. Thermal Mapping and Heat Transfer Analysis of an Induction Motor of an Electric Vehicle Using Nanofluids as a Cooling Medium. Sustainability2023, 15(10), 8124; https://doi.org/10.3390/su15108124
19. Q. Lü, X. Wang, L. Yang et al. Optimization Design and Experimental Study of Cooling System in a High Voltage Induction Motor after Power Density Upgrade. Recent Advances in Electrical & Electronic motorering, (2023). 16. https://doi.org/10.2174/2352096516666230216094059
20. A. Mengmeng, L. Wenhui, X. Ziyi Research on energy saving and

thermal management of high-efficiency and high-voltage motor based on fluid network decoupling. Energy Reports, Volume 7, 2021, Pages 8332-8345, ISSN 2352-4847, https://doi.org/10.1016/j.egyr.2021.09.106.
21. K. Hruska, V. Kindl, R. Pechanek et al. Evaluation of different approaches of mathematical modelling of thermal phenomena applied to induction motors. 10th International Conference, ELEKTRO 2014.-Proceedings, (2014) 358-362. 10.1109/ELEKTRO.2014.6848918
22. Y. Luo, L. Wang, D. Sidorov et al. An Approach to Estimate the Temperature of an Induction Motor under Nonlinear Parameter Perturbations Using a Data-Driven Digital Twin Technique. Energies, (2024). 17. 4996. https://doi.org/10.3390/en17194996
23. V. Kuznetsov, M. Tryputen, V. Tytiuk et al. Modeling of thermal process in the energy system “Electrical network - asynchronous motor”. E3S Web of Conferences. (2021) 280. 05003. https://doi.org/10.1051/e3sconf/202128005003.https://www.ansys.com/products/electronics/ansys-motor-cad
24. О. Д. Гольдберг, Я.С. Гурин, И. С. Свириденко Проектирование электрических машин. 2-е изд., перераб. и доп. М.: Высш. шк., 2001. 430 с
25. D. Staton, A. Boglietti, A. Cavagnino, Solving the More Difficult Aspects of Electric Motor Thermal Analysis, IEMDC 2003 Conference Proc. 1-4 June 2003, Madison Wisconsin, USA
26. F. Heiles, Design and Arrangement of Cooling Fins", Elecktrotecknik und Maschinenbay, Vol. 69, No. 14, July 1952

Transliterated

1. Awungabeh F.A., Besong J.E., Yasutaka F. Airflow Cooling Mechanism for High Power-Density Permanent Magnet Motor. IEEE Open Journal of the Industrial Electronics Society. (2024). pp. 1-14. https://doi.org/10.1109/OJIES.2024.3360509
2. S. Madhavan, R. Devdatta, E. Gundabattin. Thermal Analysis and Heat Management Strategies for an Induction Motor, a Review. Energies,2022, 15(21), 8127; https://doi.org/10.3390/en15218127
3. V. F. Bolyukh ,N. Kryukova, I. I. Katkov Influence of cryogenic temperature processes on the work of the linear pulse electromechanical converter // Refrigeration Science and Technology. – Vol. 2017-May, 2017, Pages 263-268
4. Ł. Nogal, A.Magdziarz, D. D. Rasolomampionona et al. The Laboratory Analysis of the Thermal Processes Occurring in Low-Voltage Asynchronous Electric Motors. Energies, (2021). 14. 2056. https://doi.org/10.3390/en14082056
5. L. Shao, A.Karci, D. Tavernini et al. Design Approaches and Control Strategies for Energy-Efficient Electric Machines for Electric Vehicles-A Review. IEEE Access. (2020), pp. 1-1. https://doi.org/10.1109/ACCESS.2020.2993235
6. O. Wallscheid Thermal Monitoring of Electric Motors: State-of-the-Art Review and Future Challenges. IEEE Open Journal of Industry Applications. (2021). pp. 1-1. https://doi.org/10.1109/OJIA.2021.3091870
7. Gundabattini, Edison & Solomon, Darius & Kalam, Akhtar & Kothari, D.P. & Bakar, Rosli. (2020). A review on methods of finding losses and cooling methods to increase efficiency of electric machines. Ain Shams Engineering Journal. 12. https://doi.org/10.1016/j.asej.2020.08.014
8. X. Li, X. Zhao, Z. Zhang et al. Selecting cooling methods for electric motors. Applied Thermal Engineering 274 (2025) 126554. https://doi.org/10.1016/j.applthermaleng.2025.126554.
9. D. Konovalov, I. Tolstorebrov, T.M. Eikevik et al. Recent Developments in Cooling Systems and Cooling Management for Electric Motors. Energies, 2023, 16(19), 7006, https://doi.org/10.3390/en16197006
10. K. Y. Reddy, P. Vamsi, R. Peram. et al. Thermal Analysis and Cooling Strategies of High-Efficiency Three-Phase Squirrel-Cage Induction Motors-A Review. Computation. (2024). 12. 6. https://doi.org/10.3390/computation12010006
11. A. Boglietti, F. Mandrile, E. Carpaneto et al. Stator Winding Second-Order Thermal Model including End-Winding Thermal Effects. Energies. (2021).14. 6578. https://doi.org/10.3390/en14206578
12. R. Selvakumar, N. Sasikumar, R. Sathish et al. Thermal Analysis of an Electric Motor in an Electric Vehicle. Conference: WCX SAE World Congress Experience. SAE Technical Papers. (2023). https://doi.org/10.4271/2023-01-0532
13. K. K. Ronnberg, M. Beniakar. Thermal modelling of totally enclosed fan-cooled motors via conjugate heat transfer analysis and air-flow measurements. Conference: 2016 IEEE Conference on Electromagnetic Field Computation (CEFC). 2016. 1-1. https://doi.org/10.1109/CEFC.2016.7816290
14. Y. Xia, B. Ren, B. Jing Et al. Analysis of transient temperature field of five-phase induction motor with composite winding under different operating conditions. Case Studies in Thermal Engineering, Volume 63, 2024, 105402, https://doi.org/10.1016/j.csite.2024.105402.
15. O. O. Badran, H. Sarhan, B. Alomour. Thermal performance analysis of induction motor. International Journal of Heat and Technology. 2012, 30(1):75-88.
16. Młot, Adrian & Korkosz, Mariusz & Lechowicz, Andrzej & Podhajecki, Jerzy & Rawicki, Stanisław. Electromagnetic analysis, efficiency map and thermal analysis of an 80-kW IPM motor with distributed and concentrated winding for electric vehicle applications. Archives of Electrical motorering, (2022). 981-1002. https://doi.org/10.24425/aee.2022.142120
17. V. F. Bolyukh, O. I. Kocherga Efficiency of multi-armature linear pulse electromechanical power and speed converters. Electrical motorering & Electromechanics, 2024, no. 3, pp. 3-10. https://doi.org/10.20998/2074-272X.2024.3.01
18. G. K. Pandey, S. S. Sikha, A. Thakur et al. Thermal Mapping and Heat Transfer Analysis of an Induction Motor of an Electric Vehicle Using Nanofluids as a Cooling Medium. Sustainability2023, 15(10), 8124; https://doi.org/10.3390/su15108124
19. Q. Lü, X. Wang, L. Yang et al. Optimization Design and Experimental Study of Cooling System in a High Voltage Induction Motor after Power Density Upgrade. Recent Advances in Electrical & Electronic motorering, (2023). 16. https://doi.org/10.2174/2352096516666230216094059
20. A. Mengmeng, L. Wenhui, X. Ziyi Research on energy saving and thermal management of high-efficiency and high-voltage motor based on fluid network decoupling. Energy Reports, Volume 7, 2021, Pages 8332-8345, ISSN 2352-4847, https://doi.org/10.1016/j.egyr.2021.09.106
21. K. Hruska, V. Kindl, R. Pechanek et al. Evaluation of different approaches of mathematical modelling of thermal phenomena applied to induction motors. 10th International Conference, ELEKTRO 2014.-Proceedings, (2014) 358-362. 10.1109/ELEKTRO.2014.6848918
22. Y. Luo, L. Wang, D. Sidorov et al. An Approach to Estimate the Temperature of an Induction Motor under Nonlinear Parameter Perturbations Using a Data-Driven Digital Twin Technique. Energies, (2024). 17. 4996. https://doi.org/10.3390/en17194996
23. V. Kuznetsov, M. Tryputen, V. Tytiuk et al. Modeling of thermal process in the energy system “Electrical network - asynchronous motor”. E3S Web of Conferences. (2021) 280. 05003. https://doi.org/10.1051/e3sconf/202128005003.https://www.ansys.com/products/electronics/ansys-motor-cad
24. Goldberg O.D., Gurin Ya.S., Sviridenko I.S. Proektirovanie elektricheskikh mashin (Design of electrical machines). Moscow: Vysshaya shkola, 2001. 430 p.
25. D. Staton, A. Boglietti, A. Cavagnino, Solving the More Difficult Aspects of Electric Motor Thermal Analysis, IEMDC 2003 Conference Proc. 1-4 June 2003, Madison Wisconsin, USA
26. F. Heiles, Design and Arrangement of Cooling Fins", Elecktrotecknik und Maschinenbay, Vol. 69, No. 14, July 1952

Надійшла (Received) 30.01.2026
Прийнята (Accepted) 16.02.2026
Опублікована (Published) 30.04.2026

Відомості про авторів / About the authors

Дзеніс Сергій Євгенович (Sergii Dzenis) **–** аспірант Національного технічного університету "Харківський політехнічний інститут", ORCID: https://orcid.org/0000-0002-8255-559X, E-mail: serhii.dzenis@ieee.khpi.edu.ua,

Болюх Володимир Федорович (Bolyukh Volodymyr) **–** доктор технічних наук, професор, Національний технічний університет «Харківський політехнічний інститут», м. Харків, Україна; ORCID ID: https://orcid.org/0000-0001-9115-7828; e-mail: vfbolyukh@gmail.com.